Collisional energy transfer probabilities of highly excited molecules from kinetically controlled selective ionization (KCSI). I. The KCSI technique: Experimental approach for the determination of P(E′,E) in the quasicontinuous energy range

Uwe Hold, Thomas Lenzer, Klaus Luther, Karsten Reihs, and Andrew C. Symonds

Citation: The Journal of Chemical Physics **112**, 4076 (2000); doi: 10.1063/1.480957
View online: http://dx.doi.org/10.1063/1.480957
View Table of Contents: http://scitation.aip.org/content/aip/journal/jcp/112/9?ver=pdfcov
Published by the AIP Publishing

Collisional energy transfer probabilities of highly excited molecules from kinetically controlled selective ionization (KCSI). I. The KCSI technique: Experimental approach for the determination of $P(E',E)$ in the quasicontinuous energy range

Uwe Hold, Thomas Lenzer, Klaus Luther,[a] Karsten Reihs, and Andrew C. Symonds
Institut für Physikalische Chemie, Universität Göttingen, Tammannstr. 6, D-37077 Göttingen, Germany

(Received 16 October 1998; accepted 27 October 1999)

The method of *kinetically controlled selective ionization* (KCSI) for investigating collisional energy transfer in highly vibrationally excited molecules is presented in detail. In this first paper of a series the focus is on the key concepts and the technical realization of KCSI experiments to provide a common basis for following reports on our available results of KCSI studies on the vibrational relaxation of a variety of larger molecules. The KCSI technique directly monitors the energetic position and shape of the population distributions $g(E,t)$ during the relaxation process by means of an energy selective two photon ionization process via an electronic intermediate state. Such measurements allow—for the first time—to extract complete and accurate experimental sets of transition probability distributions $P(E',E)$ even at quasicontinuous densities of states. Basic energy transfer quantities are already obtained from a straightforward analysis of the arrival time and width of the KCSI curves. A master equation formalism is outlined which is the basis of a data inversion providing a complete evaluation of the experimental information content. Various examples of characteristic KCSI data on collisional deactivation of highly vibrationally excited molecular populations are used to discuss important aspects of the quality and the general character of $P(E',E)$ parameters deduced from such measurements. The conditions for a successful modeling of these data are very tightly bound, and the resulting energy transfer parameters $\langle \Delta E(E)^n \rangle$ are therefore of high precision. In Paper II [J. Chem. Phys. **112**, 4090 (2000), following article] we give a full account of the toluene KCSI experiments. We will deal with our completed studies on azulene, azulene-d_8, pyrazine and pyridine in follow-up publications of this series. © *2000 American Institute of Physics.* [S0021-9606(00)01504-X]

I. INTRODUCTION

Highly vibrationally excited molecules play a key role as reactants or intermediates in important classes of thermal or photochemical reactions. Inelastic collisions with inert bath media may, e.g., provide potential reactants with energy to overcome reaction thresholds, deactivate them prior to reaction or stabilize vibrationally excited products.

Competition between reactive steps and collisional energy transfer (CET) thus determines the overall dynamics in many reactive systems. This has always been a strong motivation for a great variety of experimental studies on collisional deactivation of highly vibrationally excited molecules as well as for numerous theoretical investigations.[1–6] Nevertheless our understanding of collisional energy transfer for the high vibrational energies of chemical significance is still quite inadequate and not comparable to the level reached, e.g., in various fields of reactive collisions.

At chemically significant energies, collision induced transitions in nearly all but the smallest molecules happen within a quasicontinuum of states, in which the determination of state-to-state energy transfer quantities is practically, or even in principle no longer feasible. In this regime progressively only energy E and angular momentum J survive as ''good'' quantities to characterize the state of the excited molecule. A complete description of CET in the quasicontinuous energy range in a master equation approach therefore requires the knowledge of the *rate coefficients* $k(E',J';E,J)$ for molecules with initial energy E and angular momentum J to undergo a collision and finish at energy E' and angular momentum J'. $k(E',J';E,J)$ is usually expressed as the product of a collision number $Z(E,J)$ and a *transition probability density function* $P(E',J';E,J)$,

$$k(E',J';E,J)=Z(E,J)P(E',J';E,J). \tag{1}$$

Detailed experimental information on the dependence of energy transfer on J for large highly excited polyatomic molecules is still missing. However, trajectory calculations strongly suggest that the rotational population of an ensemble of large highly vibrationally excited molecules in a room temperature bath can be well characterized by a steady-state rotational temperature not far above 300 K which is established after a few collisions and then maintained during most of the collisional relaxation cascade.[7,8] Therefore, the energy removal from the excited molecule in standard cases of multi-step deactivation is dominated mainly by its loss of vibrational energy. In this case one can drop the J dependence and concentrate on $P(E',E)$,

[a]Author to whom correspondence should be addressed.

$$k(E',E)=Z(E)P(E',E). \tag{2}$$

$P(E',E)$ is thus the central quantity for CET which allows to determine the evolution of energy distributions during deactivation as well as the various moments of energy transfer $\langle \Delta E(E)^n \rangle$,

$$\langle \Delta E(E)^n \rangle = \int_0^\infty (E'-E)^n P(E',E)dE'. \tag{3}$$

Classical, semiclassical, and quantum mechanical studies have given important insights and revealed detailed aspects of collisional energy transfer, but nevertheless the resulting theoretical picture is still patchy.[6,9,10] In particular, there is no sufficient theoretical model available which could be directly applied to the quantitative interpretation of collisional deactivation at high densities of states at least for larger ''standard'' molecules without any ''special'' physical properties. Truly predictive theoretical capabilities appear to be even further away.

Trajectory calculations have been proved as a versatile tool for studying highly vibrationally excited molecules and represent a valuable bridge between theory and experiment.[7,8,11–19] The potential of these numerical computer simulations to test experimentally inaccessible variations of molecular parameters and to provide detailed dynamical aspects of the collision event itself has become even more promising as very recent results have shown surprisingly good quantitative agreement between classical trajectory data and corresponding full quantum scattering calculations, even for such a small molecule as CS_2.[20] However, it has also become very clear, how sensitively the results of trajectory calculations depend on the correct choice of the intermolecular potential parameters in particular.[21] Close quantitative agreement with experimental data is therefore rather an exception than the rule. In practice, a problem is faced very often with data from trajectory calculations as well as from pure theory. There are distinct results on dynamical details, quantitative trends, etc. of collisional energy transfer, which one would like to accept as granted. However, at the same time the correspondingly calculated first moments of energy transfer, $\langle \Delta E \rangle$, differ considerably from experimental values such that newly calculated systematic trends are only small effects compared with the existing mismatch in $\langle \Delta E \rangle$. In general, one can neither ignore nor really answer the question, to which extent such calculated detail would survive if eventually good general agreement with experimental data were reached. To be on the safe side such agreement concerning the fundamental $\langle \Delta E \rangle$ data are certainly a necessary condition. But even that may not be sufficient, as in the case of the so-called ''supercollisions.'' We have reported first examples of experimentally determined full and detailed $P(E',E)$ distributions including these very efficient, but rare collisions.[22] In all cases they sum up to a very small fraction (well below 1%) of all collisions and thus substantiate related estimates reported from experimental indications of ''supercollisions.''[23–28] In contrast, trajectory calculations yield in most cases much larger fractions, which would have serious consequences in practical reaction kinetics if they were real.[7,29,30]

On the experimental side, a variety of ''direct'' methods have been developed over the recent years,[4] which monitor either the energy loss of the excited molecule or the energy uptake of the collision partner. The techniques most frequently applied are ultraviolet absorption (UVA)[31–34] and infrared fluorescence (IRF).[35–41] Both methods detect an energy dependent observable of the excited molecules (e.g., an absorption coefficient ϵ or the IR emission intensity I of C–H stretching modes) which thus acts as a sort of ''internal thermometer.'' Via a calibration curve of the dependence of ϵ or I on energy, the change of these quantities during collisional relaxation can be converted into an energy loss profile describing the deactivation rate. Standard UVA and IRF methods therefore monitor a signal which is related to the cumulative response from the whole ensemble of relaxing molecules. Thus they are sensitive to the net energy removal, i.e., to $\langle\langle \Delta E(\langle E \rangle)\rangle\rangle$, the first moment of energy transfer $\langle \Delta E \rangle$ averaged over the relaxing population g with the mean energy $\langle E \rangle$,

$$\langle\langle \Delta E(\langle E \rangle)\rangle\rangle = \int_0^\infty g_{\langle E \rangle}(E')\langle \Delta E(E')\rangle dE'. \tag{4}$$

If the calibration curve is known with sufficient precision, IRF and UVA experiments can also determine the energy dependence of $\langle\langle \Delta E \rangle\rangle$. The same is valid for a variety of other methods that measure directly the ''first moment'' of energy transfer—actually $\langle\langle \Delta E \rangle\rangle$—via techniques to monitor the energy input of the bath gas, e.g., Hg tracer,[42–44] optoacoustic,[45–47] and thermal lensing experiments,[48–51] etc.

The above methods however cannot determine full $P(E',E)$ distributions. Two-color IRF experiments have been performed which yielded very limited information on higher moments as, e.g., $\langle \Delta E^2 \rangle$. So far the benzene* +benzene and pyrazine*+pyrazine systems[37,39] have been studied. A further extension of IRF techniques can be expected in applications of the newly introduced method of time-resolved Fourier transform infrared emission spectroscopy (TR-FTIRES).[52–54]

A different type of experiments extracts information by observation of the acceptor molecule in the CET process.[27,28,42–51,55–60] Flynn, Mullin, and co-workers, e.g., have used a quantum state resolved scattering technique, applying high resolution diode or F-center laser spectroscopy to study CET of highly vibrationally excited molecules, as, e.g., pyrazine, by monitoring the energy uptake of the collider.[27,28,55] Experiments have been applied to a variety of systems involving CO_2, CO, N_2O, and H_2O as acceptor molecules,[61,62] and extension to other colliders and excitation energies would be valuable. This method allows to determine very accurately a section of the tail of the downward $P(E',E)$ distribution, as it measures absolute amplitudes of $P(E',E)$ for high values of $|E'-E|$ for spectrally resolved (v,J)-states of the bath gas acceptor.

So far, experimental restrictions have prevented such direct measurements in the range of smaller ΔE where the vast majority of collisions occur.[28,57] Studies on the energy dependence of $P(E',E)$ in these single collision experiments require a corresponding variation of the excitation energy, currently in the range between 31 000 and 41 000 cm^{-1}.[58,60]

With their specific data on the role of the *V, R, T* relaxation channels such state resolved measurements on the energy accepting particle provide ideal, complementary information on CET obviously not directly available from KCSI studies on the energy loss of the relaxing donor molecules at high densities of states.

In this Paper I of our contribution, we present in some detail an experimental method which has proved to be powerful to map out complete sets of transition probability functions $P(E',E)$ for CET of various highly vibrationally excited molecules, even in an energy continuum. This technique, characterized as ''kinetically controlled selective ionization (KCSI),'' allows us to determine $\langle \Delta E \rangle$ and the higher moments of energy transfer over wide energy ranges, with high precision and accuracy. Cursory descriptions of the KCSI method and a short summary of some of our most recent results have been published previously.[22–24,63,64(a)]

In order to provide the necessary information to judge the relevance of the KCSI results on toluene (Paper II) and other systems already studied (which will be fully reported in follow-up papers of this series), we have to deal with various aspects of the method in detail. We start with the basic concepts of KCSI and show, how this method can be successfully applied to the investigation of large molecule CET. It is then outlined, how the manifold of information in the KCSI data can be exploited; approximately, by a simple ''arrival time analysis'' of the signals, and in a full manner by a master equation analysis, illustrated by representative examples from completed studies.

Paper II [J. Chem. Phys. **112**, 4090 (2000), following article][64(b)] presents a detailed KCSI study on the deactivation of highly vibrationally excited toluene by various colliders, with full experimental $P(E',E)$ data for a wide energy range and systematic results on functional dependencies of $P(E',E)$. This analysis will enable us *inter alia* to extract $\langle \Delta E \rangle$, $\langle \Delta E^2 \rangle$ and their energy dependence with high accuracy, and, e.g., to determine the importance of highly efficient collisions (frequently termed ''supercollisions''). Corresponding data on the available results of deactivation studies of highly vibrationally excited azulene, perdeuteroazulene, pyrazine, and pyridine will be presented in follow-up papers of this series.[65–69]

II. THE KCSI METHOD

A. Basic principles

In ''kinetically controlled selective ionization (KCSI)'' a pulsed laser resonant two-photon ionization is used for energy selective detection of highly vibrationally excited molecules in the electronic ground state (S_0^*). The right-hand side of Fig. 1 shows a scheme of the process.

A molecule in S_0^* is pumped into an electronic intermediate state S_n by absorption of a photon with the wavelength λ_1. The rate coefficient for this process is $k_1=\sigma_1 I_1$, given by the laser intensity $I_1(\lambda_1)$ and the absorption cross section $\sigma_1(\lambda_1,E(S_0^*))$, which depends parametrically on the internal energy E of the S_0^* molecule. Absorption of a second photon (at λ_2) is then sufficient to ionize the molecule from the intermediate state S_n with the rate coefficient

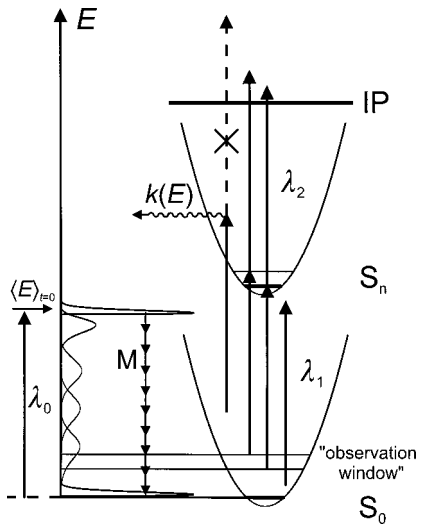

FIG. 1. Principle of the ''kinetically controlled selective ionization'' (KCSI) method for probing collisional energy transfer. A resonant intermediate state, S_n, with strongly energy dependent lifetime is chosen for two-photon ionization. Kinetic competition between an intramolecular transition, $k(E)$, e.g., an internal conversion, and further laser pumping (λ_2) limits effective ionization to a narrow energy interval in S_n (short upper gray stripe). With the choice of λ_1 a corresponding ''observation window'' is defined for the ionization of S_0^* molecules (long lower gray stripe). The lower left corner shows a cartoon of the pump step (λ_0) to prepare the initial quasi-microcanonical distribution (e.g., via internal conversion) and snapshots of the subsequent evolution of the population distribution within the electronic ground state S_0 due to the deactivation by the collider *M* which is probed by the KCSI process.

$k_2=\sigma_2 I_2$. The resulting ion yield however depends crucially on a kinetic competition between up-pumping at λ_2 and depletion of the intermediate state population through loss channels. In Fig. 1 the rate coefficient $k(E)$ represents the sum of those intramolecular processes in the S_n state, which promote a molecule into states, from which one-photon ionization at λ_2 is not possible, e.g., internal conversion, fluorescence, possibly intersystem crossing, and even predissociation.

If the rate for the loss processes is significantly faster than for the second absorption step $[k(E) \gg \sigma_2 I_2]$ ionization is effectively suppressed. In the opposite case $[k(E) \ll \sigma_2 I_2]$ the influence of the competing channels is negligible and no decrease in the ion yield is observed. Hence this *ionization is kinetically controlled* by the ratio between the energy dependent rate coefficient $k(E)$ and the value of k_2.

Suppose the lifetime τ of S_n shows a distinct energy dependence of the type that $k(E)(=\tau^{-1})$ increases very strongly above some energy not far from the origin of S_n. With a suitable choice of laser intensity I_2, efficient ionization can then be confined to the energy range of S_n with low $k(E)$ as intermediate state, while kinetic competition prevents up-pumping at all higher energies. Many molecules show this type of energy dependent lifetime distribution $\tau(E)$ in excited states S_n, and thus allow to establish such a limited energy range for resonant two- or even multistep ionization.

By the choice of wavelength λ_1 it is projected down on the energy scale of the electronic ground state. An ''*energy window*'' (or ''*observation window*'') for KCSI detection is formed with its lower edge defined by the energetic con-

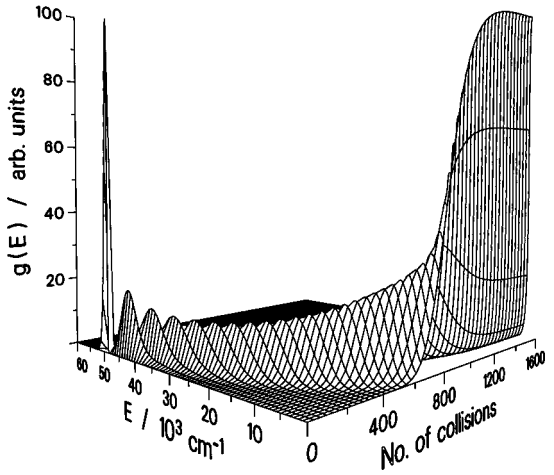

FIG. 2. Three-dimensional representation showing the evolution of an initially quasi-microcanonical population of highly vibrationally excited molecules under the influence of collisions with a bath gas *M*.

straint of the minimum vibrational energy necessary to reach the origin of S_n with a photon at λ_1 (see Fig. 1). It is important to note that the KCSI detection is *energy selective but not state selective*. It should therefore not be confused with types of state specific ''recovery spectroscopy'' which cannot conclude on the time dependent populations at defined total vibrational energies during relaxation of larger polyatomic molecules.

B. Monitoring collisional deactivation by KCSI

Figure 1 also illustrates the application of KCSI to the collisional relaxation of highly vibrationally excited molecules in a typical pump and probe scheme. At $t=0$ a narrow distribution of highly vibrationally excited molecules is generated, e.g., by ns pulsed UV laser absorption ($S_0 \rightarrow S_1$) followed by a very fast internal conversion (IC, $S_1 \rightarrow S_0$), which essentially transfers molecules with the narrow room temperature distribution up to $\langle E \rangle_0$, the starting energy for the relaxation. Subsequent collisions in a low pressure bath gas *M* then deactivate the molecules, e.g., on a μs time scale as indicated in the left corner of Fig. 1 as a ''cartoon'' by a sequence of schematic population distributions as they relax in S_0 and broaden during a cascade of collisions with *M*. The time evolution of the vibrational populations during this process is then probed in KCSI ''observation windows'' as described above. Variation of the wavelength λ_1 allows to shift the window on the energy scale, and thus to monitor the time evolution of the vibrational populations at different positions on the ground state energy scale.

The total evolution of the molecular population $g(E,t)$ in time and energy in a typical deactivation experiment is shown in Fig. 2 in a three-dimensional plot. Parallel to the energy axis cuts through the full surface are drawn for various time intervals (time is scaled in number of collisions, $Z_{LJ}[M]t$, where Z_{LJ} is the Lennard-Jones collision number[32]). They show how the initial quasi-microcanonical population distribution at a starting energy $\langle E \rangle_0 = 49\,380\ \mathrm{cm}^{-1}$ loses its energy and broadens with increasing time *t*. At the end of the deactivation process the narrow room temperature Boltzmann distribution is reached again. A sufficient series of snapshots of energy distributions—''cuts'' parallel to the energy axis at fixed times *t*—clearly contains the complete information of the $g(E,t)$ surface.

KCSI curves are now simply ''cuts'' orthogonal to the previous ones; they dissect the $g(E,t)$ surface at fixed energies *E* along the time axis *t*. The information content of a sufficient series of KCSI curves is thus totally equivalent to that of a series of measured energy distributions at various times *t*. This is immediately clear from Fig. 2, when viewing onto the number-of-collision axis (from the right side). The lines parallel to this axis refer to transient KCSI ion signals, as one would observe when having an δ-function shaped observation window at the corresponding energy. For the energy window at the lowest energy ($E=0$) the maximum ion signal is obtained after complete deactivation. Transient ion signals for windows at higher energies appear clearly earlier, as it takes less time to build up population at these energies of observation. At high lying observation windows complete passage of the relaxing molecular population is observed. After having reached a maximum value, the ionization signal practically disappears. At low observation energies after long times a constant fraction of the thermal Boltzmann distribution $f(E)$ extends into the observation window after complete relaxation. Thus residual ionization yields decrease for observation windows at increasingly higher energies corresponding to the exponential ''Boltzmann tail.''

C. A representative example: KCSI observation of azulene* relaxation in *n*-heptane

At this point we want to illustrate the technical reality and the capabilities of the KCSI method by one representative example, the deactivation of highly vibrationally excited azulene molecules by *n*-heptane. A cursory overview of our KCSI study on CET phenomena in the azulene system can be found in Ref. 22 and a much more detailed description of the results will be given in the follow-up Paper III of this series.[65–67]

Figure 3 shows experimental KCSI signals for the system under consideration. Six independent curves from measurements at three different observation windows (wavelength $\lambda_1 = 365$ nm, 355 nm, and 350 nm, corresponding to a mean energy of the optimized observation windows of $E_{\mathrm{center}} = 5910$, 4720, and 2930 cm^{-1}, respectively) and two different excitation energies (wavelength $\lambda_0 = 532$ nm and 337 nm, producing nascent vibrational populations with $\langle E \rangle_0 \approx 19\,780\ \mathrm{cm}^{-1}$ and $30\,650\ \mathrm{cm}^{-1}$, respectively) have been obtained. The lines represent a fit from a master equation analysis of the experiments by using a monoexponential transition probability $P(E',E)$ with parametric exponent in the argument for various colliders (see Sec. III B and Paper II for details).

The upper half of Fig. 3 shows the KCSI ''snapshots'' for the deactivation of azulene molecules starting at an initial energy of $19\,780\ \mathrm{cm}^{-1}$. The window for $\lambda_1 = 365$ nm is the highest lying one on the energy scale. For this reason its signal shows the earliest rise. The second and third signal rise increasingly later in time because they belong to obser-

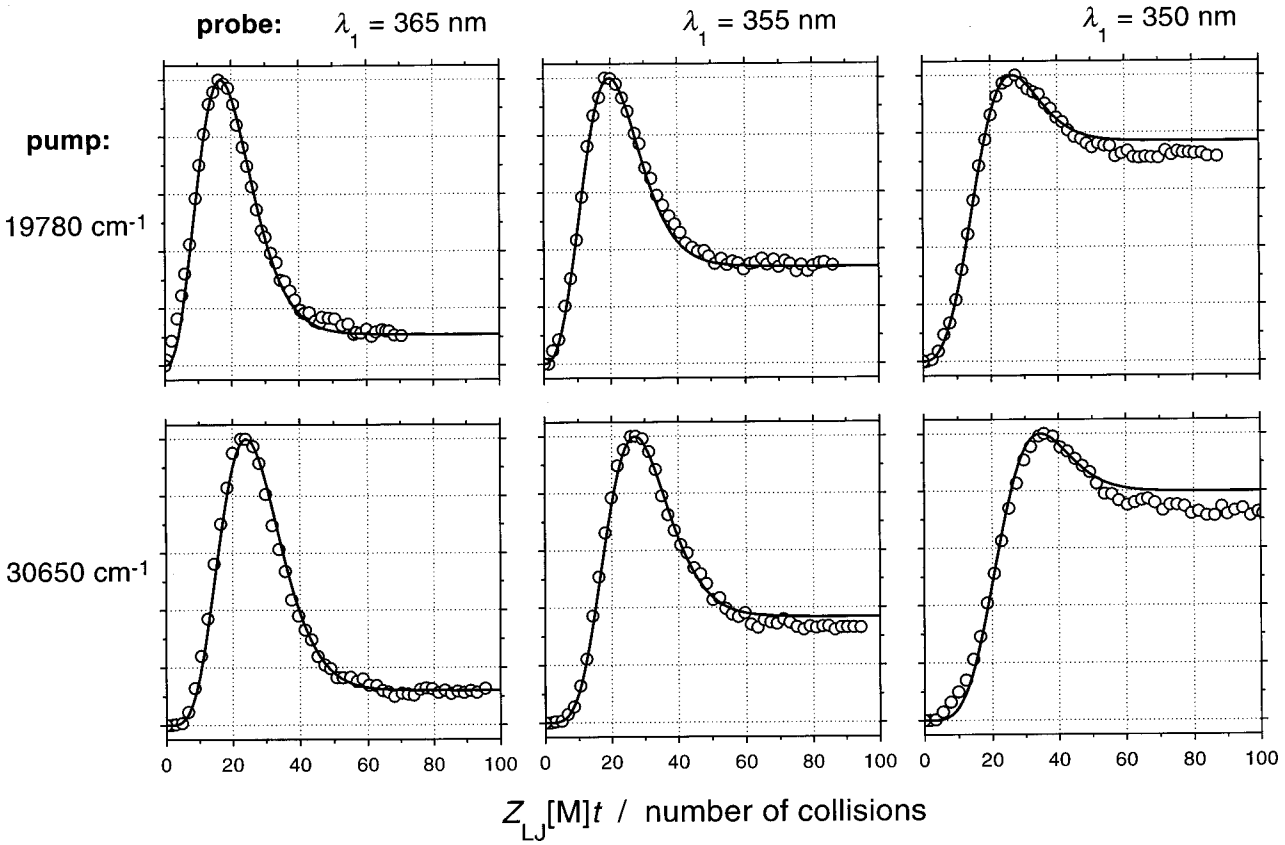

FIG. 3. KCSI data for the deactivation of highly vibrationally excited azulene by *n*-heptane. Two different excitation energies, 30 650 cm^{-1} ($\lambda_0 = 337$ nm) and 19 780 cm^{-1} ($\lambda_0 = 532$ nm), three different observation windows, $\lambda_1 = 365$ nm, 355 nm, and 350 nm (mean observation window energy $E_{center} = 5910$, 4720, and 2930 cm^{-1}). The lines represent an optimized fit obtained from a master equation analysis using a monoexponential transition probability with parametric exponent Y of the form $P(E',E) \propto \exp[-((E-E')/\alpha_1(E))^Y]$ with energy dependent parameter $\alpha_1(E)/cm^{-1} = 645 + 59.5 \times 10^{-3} \cdot E$ and $Y = 1.2$; for details, see text.

vation windows at energetically lower positions on the energy scale. The characteristic difference in the rise time of the signals results from the additional time needed for the excited molecules to lose the energy which corresponds to the difference between the respective observation windows. Another important feature is the width of the KCSI signals which is directly correlated with the width of the distributions passing the observation window. Finally, the variation in the residual ion signal at long times should be noted which reflects the portion of the thermal Boltzmann distribution $f(E)$ inside the observation window after complete deactivation as mentioned above.

In the lower half, the signals for the same observation windows are shown, *but* for azulene molecules starting at a higher excitation energy ($\approx 30\,650$ cm^{-1}). It is immediately clear that all signals rise at later times and have different shapes, but show an analogous dependence on the three windows as mentioned above.

Without going into details at this point, one can easily imagine, that it is a nontrivial task to model these six independent curves of complicated functional shape with a common set of parameters for the transition probability $P(E',E)$. However, the result may thus be very specific (see Sec. VI).

III. QUANTITATIVE DESCRIPTION OF KCSI SIGNALS

As discussed in the foregoing section, the resonant two color (1+1) KCSI ionization process allows us to *selectively* ionize excited molecules in the electronic ground state having a vibrational energy within a well-defined observation window. The ion signal $I_D(t)$ of the KCSI process at a specific time can therefore be represented as

$$I_D(t) \propto \int_0^\infty g(E,t) W(E,\lambda_1,\lambda_2) dE, \tag{5}$$

where $g(E,t)$ is the time dependent population g at energy E and time t, and $W(E,\lambda_1,\lambda_2)$ is the function describing the observation window for the probe wavelengths λ_1 and λ_2 at energy E.

A. The observation window function $W(E,\lambda_1,\lambda_2)$

The actual shapes of the window functions $W(E,\lambda_1,\lambda_2)$ for KCSI detection are determined by three photophysical parameters, two absorption coefficients and the lifetime of the intermediate state—all energy dependent—which are measurable in independent experiments. Of course such information is not always present in the literature with the desired detail and precision. The obvious question, how much detail in these data is needed for KCSI measurements

and what are systematic influences of the window parameters will be discussed partly here and in much more detail in Paper II.

However, there is an alternative elegant approach to this problem: The information content with respect to the window functions is also contained in the KCSI signals themselves [see Eq. (5)]. KCSI curves in deactivation experiments are mathematically very complex functions—not, e.g., simply monotonic curves—(see, e.g., Fig. 3) and allow us to evaluate a large amount of parametric information. In fact, the information from the underlying unique collisional dynamics of a relaxation process observed at, e.g., *six* windows (Fig. 3) in experiments with various collider gases of widely different CET efficiency and the additional variation of the initial excitation energies can provide such an extended basis, that the complete modeling with a master equation analysis allows to extract not only the $P(E',E)$ parameters but also the specific shape of the window function directly from the KCSI curves, as, e.g., achieved in deactivation experiments of azulene. In other words, the experiments are ''*self-calibrating,*'' [22] i.e., the data evaluation does *no longer* depend on the quality of externally determined molecular input parameters and/or derived or predicted forms of ''calibration curves'' as it is usual in CET experiments. In fact it could be demonstrated that the window functions obtained ''automatically'' (via self-optimization) by the computer during a master equation analysis of the KCSI data show the expected very close agreement with calculated ones obtained *a priori* from a procedure described in the following, on the basis of independently measurable molecular parameters.

The window function can be described by a simple model function along the lines indicated by the kinetic scheme in Fig. 1. At the laser intensities in our experiments effects like stimulated emission or nonlinearities due to the depletion of the population of excited molecules in the electronic ground state are not relevant. Furthermore, pressures are always in a range where collisions within the duration of the laser pulse (~20 ns or less) can be safely neglected. It has been demonstrated, that under such conditions N_{ion}, the number of ions produced by the two-photon KCSI process, shows the following dependence on the rate coefficient $k(E)$ of the loss processes in the intermediate state,[70]

$$N_{\mathrm{ion}} \propto \tfrac{1}{2}[1+(k(E(S_n^*))\cdot\tau_{\mathrm{eff}})^{4/3}]^{-3/4}. \tag{6}$$

τ_{eff} is an effective pulse width, which is a function of the time dependent intensity $I(t)$ and the fluence F of the laser pulse,

$$\tau_{\mathrm{eff}}=\left[2\int_{-\infty}^{+\infty}\left(\frac{I(t)}{F}\right)^2 dt\right]^{-1}. \tag{7}$$

For a Gaussian shaped pulse one obtains

$$\tau_{\mathrm{eff}}=\sqrt{\frac{\pi}{8\ln 2}}\,\tau_{\mathrm{FWHM}}\approx 0.753\tau_{\mathrm{FWHM}}, \tag{8}$$

where τ_{FWHM} is the full pulse width at half-maximum. Furthermore, it was shown that N_{ion} is nearly insensitive to the exact temporal intensity profile of the laser pulse and that one can therefore take the experimental FWHM pulse widths, at least for the standard types of lasers such as used in our experiments. The final expression for the window function resulting from Eq. (6) is

$$W(E(S_0^*),\lambda_1,\lambda_2)=\tfrac{1}{2}\sigma_1(\lambda_1,E(S_0^*))\sigma_2(\lambda_2,E(S_n^*))\times[1+(k(E(S_n^*))\cdot\tau_{\mathrm{eff}})^{4/3}]^{-3/4}. \tag{9}$$

The shape of $W(E,\lambda_1,\lambda_2)$ is therefore dictated by the energy dependence of the absorption cross sections σ in both the S_0 and S_n state and the rate constant k for the loss processes. $E(S_n^*)$ is defined as follows:

$$E(S_n^*)=E(S_0^*)+\frac{hc}{\lambda_1}-E_{0-0}, \tag{10}$$

where E_{0-0} corresponds to the energetic origin of the $S_n \leftarrow S_0$ transition. In the KCSI investigations for toluene a one-color KCSI process was used ($\lambda_1=\lambda_2$). The intermediate state in this specific case is S_1. Thus Eq. (9) transforms into

$$W(E(S_0^*),\lambda_1)=\tfrac{1}{2}\sigma_1(\lambda_1,E(S_0^*))\sigma_2(\lambda_1,E(S_1^*))\times[1+(k(E(S_1^*))\cdot\tau_{\mathrm{eff}})^{4/3}]^{-3/4}. \tag{11}$$

Figure 4 shows window functions for toluene calculated by this prescription. For further details on the calculation of the cross sections σ_i and the rate coefficient k see Paper II (following article). The sharp lower cutoff for each window occurs at the energy $E_{0-0}-hc/\lambda_1$. The shape of the high energy wing is mainly determined by the energetic dependence of k. If k increases rapidly with E one gets a rather steep decrease of the window, whereas for a smoother increase of k a much slower decrease is observed.

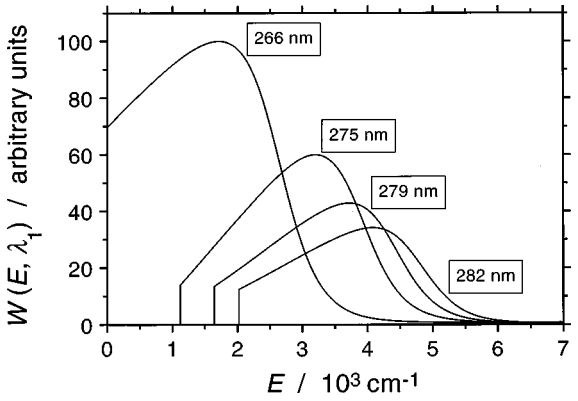

FIG. 4. Observation windows for toluene calculated via Eq. (11). λ_1 = 266 nm, 275 nm, 279 nm, and 282 nm. For a further discussion, specific parameters and the necessary modifications to obtain the optimized window functions see Paper II (following article).

B. Time evolution of $g(E)$ from a master equation formalism

The KCSI signal—and thus the shape of $g(E)$—is governed by the distinct functional dependence of the collisional transition probability $P(E',E)$. There is no way to extract an unique form for $P(E',E)$ by direct deconvolution of Eq. (5). Instead, the parameters of given functional forms for $P(E',E)$ must be determined by a ''forward'' fitting proce-

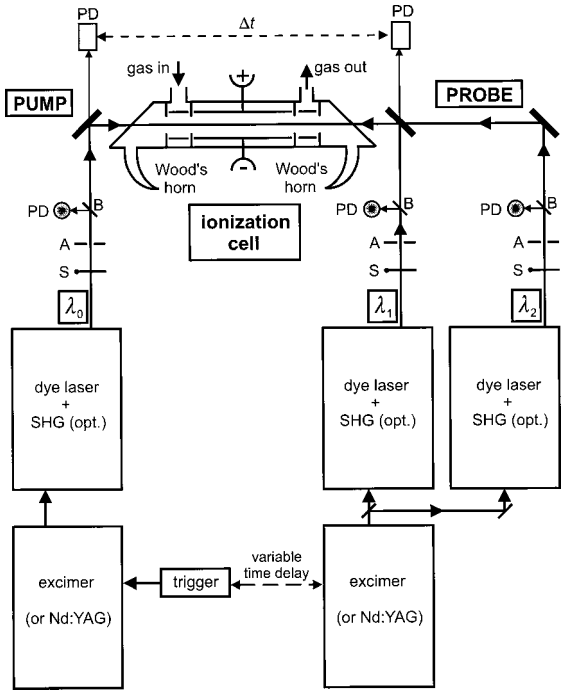

FIG. 5. General setup for a typical KCSI experiment. PD=photodiode, A=aperture, S=shutter, B=beamsplitter, SHG=second harmonic generation crystal. For details, see text.

dure for which we use a master equation analysis. Specific details of our implementation can be found in standard references.[4,71] Briefly, assuming ''detailed balance'' $[P(E',E)\cdot f(E)=P(E,E')\cdot f(E')]$ the master equation in its continuous form can be written as

$$\frac{dg(E,t)}{d(Z[M]t)}=\frac{f(E)}{c(E)}\int_0^E\frac{M(E',E)}{f(E')}\,g(E',t)dE' + \int_E^\infty\frac{M(E,E')}{c(E')}\,g(E',t)dE'-g(E,t), \tag{12}$$

where $M(E',E)=P(E',E)\cdot c(E)$ is a model function for the transition probability (e.g., exponential, biexponential,...), $c(E)$ is an energy dependent normalization constant, which can be found by standard prescriptions as given in Refs. 72 and 73, and $f(E)$ is the vibrational Boltzmann distribution. For toluene, $f(E)$ was calculated via the semiclassical expression of Whitten and Rabinovitch[74,75] for the density of states using the well-known experimental frequencies and rotational constant of the free rotor.[76,77] Comparison with an exact count of states based on the Beyer–Swinehart algorithm[78,79] yielded practically identical results at higher energies and showed differences only at the very lowest energies.

To solve Eq. (12) we used the finite-difference representation,

$$\frac{dg(j\cdot\delta E,t)}{d(Z[M]t)}=\dot g_j=\delta E\left(\frac{f_j}{c_j}\sum_{i=0}^{j}{}'\,\frac{g_i}{f_i}\,m_{ij}+\sum_{i=j}^{n}{}'\,\frac{g_i}{c_i}\,m_{ji}\right)-g_j \tag{13}$$

with the abbreviations

$$p_j=f_j/c_j,\quad h_j=g_j/f_j,\quad l_j=g_j/c_j. \tag{14}$$

The system of n ordinary differential equations (ODEs) (13) can then be reformulated in vector notation,

$$\dot{\mathbf{g}}=\delta E(\mathbf{p}\cdot\mathbf{s}+\mathbf{t})-\mathbf{g}. \tag{15}$$

$\mathbf{s}$ and $\mathbf{t}$ represent n-dimensional vectors of the (extended trapezoidal) sums Σ' in Eq. (13). The jth elements of the vectors of these sums can be written as

$$s_j=\frac{h_0}{2}\,m_{0j}+h_1m_{1j}+h_2m_{2j}+\cdots+h_{j-1}m_{(j-1)j}+\frac{h_j}{2}\,m_{jj},$$
$$t_j=\frac{l_j}{2}\,m_{jj}+l_{j+1}m_{j(j+1)}+l_{j+2}m_{j(j+2)}+\cdots+l_{n-1}m_{j(n-1)} + \frac{l_n}{2}\,m_{jn}. \tag{16}$$

For the numerical integration of Eq. (15) every single time or collision increment requires a repeated evaluation of the right-hand side (RHS) of the ODE system. The calculation of the sums in Eq. (16) is time consuming but there are strategies to overcome this problem.

For large values of $|E'-E|$ ''realistic'' transition probabilities, e.g., qualitatively similar to some exponential type,

$$P(E',E)=\frac{1}{c(E)}\exp\left[-\left(\frac{E-E'}{\alpha(E)}\right)\right] \tag{17}$$

decrease very rapidly and approach zero. $P(E',E)$ represents a two dimensional matrix. The band width of this matrix (i.e., the number of relevant elements near the diagonal) depends on the grain size δE and especially on the parameter α. As realistic values for α are much smaller than the energy interval of the complete collisional deactivation, the band width of the matrix is quite narrow. This allows us to reduce the summation limits for normalization and especially on the right-hand side of the master equation (13) considerably without sizable loss in accuracy.

In all calculations a typical grain size of $\delta E=20\,\mathrm{cm}^{-1}$ was used, as it was also for the window functions. The convergence with respect to grain size was systematically tested against calculations using $\delta E=10\,\mathrm{cm}^{-1}$, with ''worst case'' deviations being less than the line widths of the simulations shown in Fig. 3. This very good convergence is easily understood, because even for the least efficient colliders δE was always considerably smaller than the parameter α in the transition probability. Finally, contributions resulting from toluene*-CHT collisions need not to be considered in the master equation simulations because the CHT/bath gas mixing ratio in the experiments is extremely low (see Sec. IV A).

IV. EXPERIMENTAL SETUP

A. Overview

A general experimental scheme can be found in Fig. 5. In the *pump* step (wavelength λ_0) highly vibrationally excited molecules in the electronic ground state are generated by electronic absorption and subsequent fast, collision-free internal conversion. Specifically, for the preparation of the highly excited toluene molecules via the isomeric precursor 1,3,5-cycloheptatriene (see Paper II for more details) a dye

laser was used, pumped by an excimer laser at 308 nm. The resulting pulses at 532 nm were frequency doubled, yielding typical energies of 1–2 mJ at the pump wavelength $\lambda_0 = 266\,\text{nm}$, while the fundamental wavelength was either blocked by a filter or deflected by a Pellin–Broca prism. In some of the experiments a frequency quadrupled Nd:YAG laser was used to generate λ_0.

After a time delay (typically 0–10 μs) the collisional deactivation process is detected by the two-color two-photon KCSI process (wavelength λ_1 and λ_2, *probe*). This can be achieved by two dye lasers, which are pumped by a single excimer or Nd:YAG laser. For the toluene measurements however a simpler setup is possible, because the energetics allow to use a one-color two-photon ionization for KCSI detection ($\lambda_1 = \lambda_2$). As for the pump pulse an excimer pumped dye laser delivered probe pulses of up to 10 mJ (coumarine 307 or rhodamine 6G dyes). Second harmonic generation resulted in typical energies of about 1 mJ at $\lambda_1 = \lambda_2 = 266,...,282\,\text{nm}$.

The pump laser beam and the two temporally and spatially overlapping probe laser beams (a single probe beam in the specific case of the toluene experiments) are counterpropagated on the same central axis through the ionization cell which is described below. Central parts of the laser beam profiles were selected by apertures, in the case of the toluene measurements with a diameter of 1.2 mm and 3.0 mm for pump and probe, respectively.

Electric shutters are used for blocking individual laser beams in programmed standard routines to measure the ion yields resulting from any single laser or possible combinations of three (or—in the toluene setup—two) laser pulses. This is necessary for precise extraction of the ion yield of the ''pure'' KCSI process via fully controlled difference measurements (details see Sec. IV D).

The laser pulse energies can be adjusted with suitable filter arrangements and are detected by photodiodes or photomultipliers which monitor the laser pulse energies shot-to-shot. Optionally, the homogeneity of the beams can be optimized using 1:2 Galilei telescopes. Typical pressures inside the ionization cell (described in more detail in Sec. IV B) range from 1 mbar (for efficient colliders like, e.g., *n*-heptane) to 15 mbar (for inefficient colliders like, e.g., helium) and are kept constant during the experiment. Note that diffusion of excited toluene molecules from the excitation volume is completely negligible within the delay time between the pump and probe pulses when using these pressure conditions and the above beam diameters.

The sensitivity of the ion cell used in our experiments (detection limit of roughly 100 ions, see below) made it possible to use extremely small amounts of CHT in the gas mixture. Therefore no corrections for toluene*-CHT collisions were necessary, because the CHT partial pressure was extremely low [$p(\text{CHT})/p(\text{collider}) < 10^{-5}$]. This can be compared, e.g., with values of $p(\text{CHT})/p(\text{collider}) > 8 \times 10^{-3}$ and $p(\text{toluene})/p(\text{collider}) > 1.2 \times 10^{-2}$ reported in Refs. 32 and 80, respectively. We checked the composition of our mixtures routinely by UV spectroscopic analysis. In addition, deliberately increasing the CHT partial pressure, e.g., by a factor of two had no influence on the shape of the experimental KCSI curves, unambiguously showing that collisional deactivation by CHT did not affect the observed signals. The low CHT partial pressure together with a typical excitation of less than 10% of the molecules also means that the temperature increase of the gas sample is negligible (in all cases <1 K).

In the following we discuss in more detail how the KCSI ion signal is measured and what corrections are necessary to account for fluctuations in the concentrations and laser energies.

B. Ionization cell

The homebuilt ionization cell—constructed of stainless steel high vacuum components—is the central part of the setup (for a very schematic overview, see Fig. 5). On the two ends facing the incoming beams, quartz windows are mounted on Viton O-rings at 45° to the optical axis. Collector and guard electrodes are mounted on a Teflon block, which is positioned centrally within the chamber. The middle electrodes, the collector plates ($10 \times 64\,\text{mm}^2$), which are symmetrically biased with voltages of $+80$ V and -80 V, register the photoionization current, whilst the adjacent guard electrode pairs ($10 \times 21\,\text{mm}^2$) on both sides, kept on the same potentials, serve to eliminate uncontrolled signal contributions from outside the defined condenser arrangement and from possible photoionization events of molecules adsorbed on the windows.

When detecting the typically small photoionization signals, very minor amounts of scattered light can be a serious source of error mainly due to efficient surface-enhanced ionization of molecules adsorbed on the collector plates.[63] For the effective elimination of the influence of spurious scattered light on the electrodes an optimized set of four blocking apertures inside the cell is employed together with Wood's horns light traps which completely absorb reflections at the inner window faces as the beams leave the chamber.[63]

The ion yield is determined as follows: The current (corresponding to the total charge deposited on the collector plates during a time interval following ionization) is fed into a low-noise floating-ground differential current amplifier, which consists of a current-to-voltage converter coupled to an unit gain difference amplifier. Integration of the output voltage pulse is performed with an inverting integrator. The integrator output signal itself is further processed by an A/D converter and read out by the microcomputer. Special extended electrical shielding measures are taken in the design and layout of the measurement electronics to ensure the absence of even very small fluctuations in the electrode potentials.

Calibration of the amplifier/integrator unit is achieved as follows: Applying a square wave voltage pulse of well-defined duration and amplitude via a known calibration resistor deposits a calculable charge on the (uncharged) collector plates. Measurement of the resulting integrator output voltage for a variety of such square wave pulses allows to directly connect the output voltage to the absolute number of ions collected on the plates.

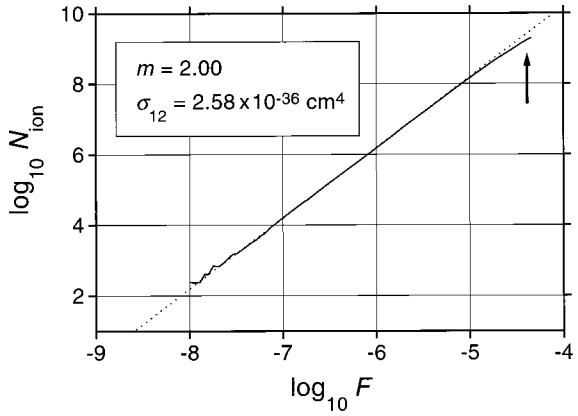

FIG. 6. Fluence dependence of the ion yield for the resonant (1+1)-photon ionization of toluene at 266.05 nm. A pure quadratic dependence is observed for yields from about 10^2 up to approximately 5×10^8 ions—as expected for an unsaturated two-photon process. The cross section of $\sigma_{12}=2.58\times10^{-36}\,\mathrm{cm}^4$ (dotted fit line) is in good agreement with the value determined in Ref. 82. At higher ion yields a leveling-off is observed (marked by the black arrow), explainable by recombination losses due to space charge effects. $P=57.3$ mbar, laser beam diameter 3 mm.

The sensitivity of the detection electronics can be tested, e.g., by measuring the dependence of the ion yield of an unsaturated two-photon process. The ionization yield at low fluences for such a case is well described by

$$\frac{N_{\mathrm{ion}}}{N_0}=\frac{\sigma_1\sigma_2}{2}F^2=\frac{\sigma_{12}}{2}F^2, \tag{18}$$

where N_{ion} is the number of ions generated during this process and N_0 the total number of molecules.[81] σ_1 and σ_2 are the absorption cross sections for the first and second photon, and F is the laser fluence. The effective two-photon ionization cross section is denoted as σ_{12}.

The resonant 1+1 ionization of toluene at 266.05 nm may serve as an example, for which the two-photon ionization cross section and the saturation intensity is well known ($\sigma_{12}=2.7\times10^{-36}\,\mathrm{cm}^4$ and $I_{\mathrm{sat}}=83\,\mathrm{MW\,cm}^{-2}$, respectively[82,83]). In Fig. 6 a typical outcome of such an experiment is shown. A well-defined quadratic dependence of the ion yield on the laser fluence is observed for yields from 10^2 (!) up to about 5×10^8 ions—as expected for an unsaturated two-photon process. However, at the highest ion yields/laser fluences a weakening of the quadratic dependence is found. This can be explained by space-charge limited recombination losses.[82] Saturation of either of the optical transitions can be safely ruled out because the maximum intensity of the laser (about 10 $\mathrm{kW\,cm}^{-2}$ in this case) is several orders of magnitude less than the saturation intensity noted above. The two-photon ionization cross section of $\sigma_{12}=2.58\times10^{-36}\,\mathrm{cm}^4$ extracted from Fig. 6 agrees very well with the value determined in Ref. 82. If lower pressures are applied (<57 mbar) one finds essentially the same behavior. In these cases the leveling-off behavior is observed at even higher ion yields. This clearly demonstrates that the ionization cell used in our investigations can accurately determine the absolute number of photoions *over more than six orders of magnitude* and wide pressure ranges.

The ionization cell itself is connected to a vacuum system which is constructed of high vacuum components sealed with Viton O-rings or aluminum seals. For cleaning purposes, the whole setup can be heated and evacuated via a turbomolecular pump backed by a two-vane oil-sealed rotary pump down to pressures as low as 10^{-7} mbar. A liquid-nitrogen-cooled foreline trap prevents pump oil from backstreaming and also freezes out substances flowing from the cell.

During the measurement the turbomolecular pump is isolated and the rotary pump, throttled by a needle valve, draws the toluene/collider gas mixture slowly through the chamber. For a typical working pressure of about 1 mbar the contents of the chamber are effectively renewed every 20 s. The pressure inside the cell is monitored by two capacitance manometers [MKS Baratron 220 B (up to 1.3 mbar) and 222 B (up to 100 mbar)].

For obtaining stable vapor pressures solid or liquid substances, as, e.g., 1,3,5-cycloheptatriene (which is used as a precursor for preparing highly excited toluene molecules, see Paper II) or collider gases like *n*-heptane, are stored in thermostatted Pyrex ampules. They are fed via needle valves into the chamber. All other collider gases are fed via a mass flow controller (Tylan FC 260 2SLM HE).

The chemical substances used for the toluene measurements were commercially available; helium, argon, and CO_2 from Messer–Griesheim, xenon from Linde; *cis*-2-butene, 1,3,5-cycloheptatriene (CHT), cyclohexane, cyclopropane, *n*-heptane and *n*-pentane from Merck, and cyclohexene, hexafluorobenzene from Aldrich. The CHT samples were carefully distilled to remove residual impurities and were stored in the dark at 253 K. All liquid colliders were thoroughly degassed by several freeze–pump–thaw cycles. The other substances were used without further purification.

C. Extraction of the time-dependent KCSI ion signal $I_D(t)$

In addition to the ion signal of the two-photon KCSI process, $I_D(t)$, a certain background of ions is also produced by sequential absorption during the laser pulses at λ_0, λ_1, and λ_2. In a typical KCSI experiment a subtraction scheme must therefore be applied which we here discuss for the specific case of toluene ($\lambda_1=\lambda_2$).

Nonresonant two-photon excitations are completely negligible at the low laser intensities in our experiments. As we prepare the vibrationally hot toluene starting from CHT instead of ''cold'' toluene (see Paper II) this has the advantage of a very low level of background ions I_0 (excitation pulse λ_0) and I_1 (detection pulse λ_1), due to the extremely small ionization cross section of CHT (see Paper II). An improved signal quality is thus achieved (Fig. 7). Nevertheless, the number of background ions, I_0 and I_1, were very carefully determined by a procedure in which each series of shots measuring a single KCSI data point was embedded in sequences of reference measurements with only one of the laser wavelengths alternatively (see below). $I_D(t)$ is then determined from the total signal at KCSI conditions, $I_{\mathrm{tot}}(t)$ by

$$I_D(t)=I_{\mathrm{tot}}(t)-I_0-(1-\eta)I_1. \tag{19}$$

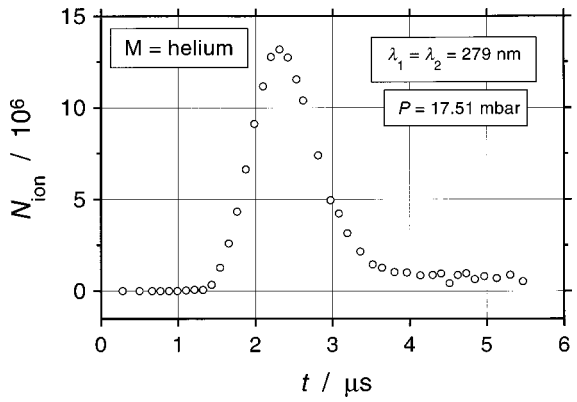

FIG. 7. Outcome of a single KCSI measurement for the deactivation of highly vibrationally excited toluene by the collider helium. The absolute ion yield of the KCSI process as a function of the delay time t between the pump and probe lasers is shown. Pump, $\lambda_0 = 266$ nm; probe, $\lambda_1 = \lambda_2 = 279$ nm ($E_{\text{center}} = 3648\ \text{cm}^{-1}$); $P = 17.51$ mbar.

η is the fraction of molecules excited in the pump pulse which was $\leqslant 10\%$. At the especially low value of I_1 for these experiments in CHT the approximation $(1-\eta) \approx 1$ was used in practice within the very minor I_1 correction. In cases where KCSI detection needs a two-color process, e.g., in our experiments with highly vibrationally excited azulene,[22,64–67] similar but more elaborate difference measurement schemes are used to accurately determine the KCSI signal $I_D(t)$.

D. Changes in concentrations and laser energies

Fluctuations in the measured ion numbers due to variations in the CHT concentration during the experiment were minimized below practical significance by careful control of the sample temperatures and sufficient premeasurement times to establish true steady-state flow conditions. However, short time fluctuations or long term drift effects of the laser energies were more difficult to eliminate. A first step in the reduction of such effects consisted in discrimination of the laser energies, omitting shots with $\geqslant 5\%$ deviation from an average energy value measured at the start of the experiment.

Some shot-to-shot fluctuations of the laser energies are inevitable. The corresponding variations of the multiphoton ion signals scale with a power of the laser pulse energy and can be described by an expression

$$I_n = k_n \cdot E_n^{m_n}, \quad (n = 0,1), \tag{20}$$

with constant parameters k_n and m_n within the relevant fluctuations of laser pulse energies E_n. Before every single pump–probe measurement, I_0 and I_1 were again determined separately with the laser pulses at λ_0 and λ_1, respectively, in up to 50 shots, as during the measurements of $I_{\text{tot}}(t)$ under pump–probe conditions. For an optimized power dependent background correction, these actual data on I_0 and I_1 were not used in an averaged way, but from each series of I_0, I_1 data a corresponding set of least square fitted parameters k_n and m_n was determined and then used to apply the ''background correction'' for each of the immediately afterwards measured pump-probe values $I_{\text{tot}}(t)$, according to the individual laser energies E_0 and E_1 monitored simultaneously. Averaging took place after this individual *in situ* evaluation of

$$I_D(t) = I_{\text{tot}}(t) - k_0 E_0^{m_0} - k_1 E_1^{m_1}. \tag{21}$$

The consistency of automatically evaluated parameters k_n and m_n within series of measurements of such type was checked by additional inspection to identify abnormal situations. In addition, every seventh measurement with various pump–probe delay times Δt was again taken at a fixed reference value of Δt to verify the consistency of experimental conditions during a total experimental period of typical 20–60 min duration. The whole measurement cycles were controlled by an AT 286 microcomputer with IEEE-488 interface logic which also read out the ion signal, energy, and pressure data. The experiment typically operated at 5 Hz.

An experimental KCSI signal obtained this way for the deactivation of highly vibrationally excited toluene by helium can be found in Fig. 7 [excitation wavelength $\lambda_0 = 266$ nm, probe wavelength $\lambda_1 = \lambda_2 = 279$ nm ($E_{\text{center}} = 3648\ \text{cm}^{-1}$)]. The measured absolute KCSI ion yield is plotted as a function of the delay time between the pump and probe lasers. The signal has a remarkably high signal to noise ratio due to the nearly background free conditions already mentioned before. All in all, typically one to five of such experiments were carried out under equal pump–probe conditions. The signals obtained were normalized to the same maximal $I_D(t)$ value, put onto a reduced time scale—in ''numbers of collisions''—and averaged.

For the purpose of data reduction and as a convenience for the discussion of the results in Papers I and II a dimensionless time scale in ''number of collisions,'' $Z_{\text{LJ}}[M]t$, is used for all our data, with Z_{LJ} the Lennard-Jones (LJ) collision number as reference, and $[M]$ is the number density of the bath gas in the measurements which were taken at various pressures. The collision numbers used for toluene relaxation are found in Table I, together with the corresponding effective LJ well depths ϵ_{LJ} and radii σ_{LJ}. LJ collision numbers were calculated as described in Ref. 32. Missing data for ϵ_{LJ} and σ_{LJ} of individual substances were determined either

TABLE I. Lennard-Jones potential parameters and collision numbers for collisions between toluene and the collider gas M; see Refs. 32 and 24 for details.

M	σ_M (Å)	ε_M/k_B (K)	$Z_{\text{LJ}}(10^5\ \text{Pa}^{-1}\ \text{s}^{-1})$	$Z_{\text{LJ}}(10^{-10}\ \text{cm}^3\ \text{s}^{-1})$
He	2.55	10.22	1.650	6.834
Ar	3.47	113.5	1.088	4.506
Xe	4.05	230	1.050	4.349
CO_2	3.94	201	1.335	5.530
c-propane	4.63	299	1.718	7.116
c-hexane	5.78	394	1.845	7.642
cis-2-butene	5.27	312	1.778	7.364
c-hexene	5.78	400	1.860	7.704
n-pentane	5.85	327	1.853	7.675
HFB	5.83	444	1.148	4.755
n-heptane	6.65	351	1.973	8.172
toluene	5.92	410	1.868	7.737

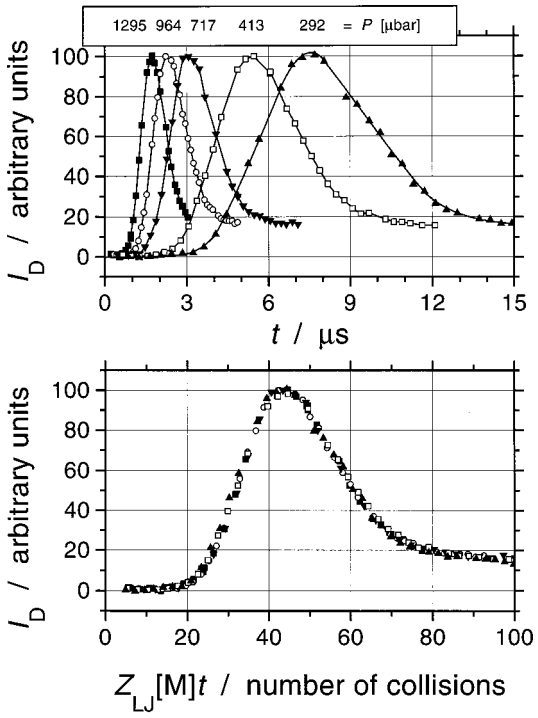

FIG. 8. Pressure dependence of the KCSI ion signal I_D for the deactivation of highly vibrationally excited toluene by *n*-heptane [pump wavelength $\lambda_0 = 266$ nm; probe wavelength $\lambda_1 = \lambda_2 = 275$ nm ($E_{center} = 3041\ cm^{-1}$)]. The upper plot shows individual KCSI signals measured at various pressures (the lower the pressure the longer the deactivation time). The lower plot is obtained by scaling the time axis with the pressure (number density) of the bath gas and the LJ collision number Z_{LJ} (Table I) yielding the average number of collisions ($Z_{LJ}[M]t$) experienced at time *t*. All curves now fall on top of each other. I_D represents the ion yield N_{ion} of the KCSI process normalized to a value of 100 at its maximum. Lines in the upper plot are intended only as a guide for the eye.

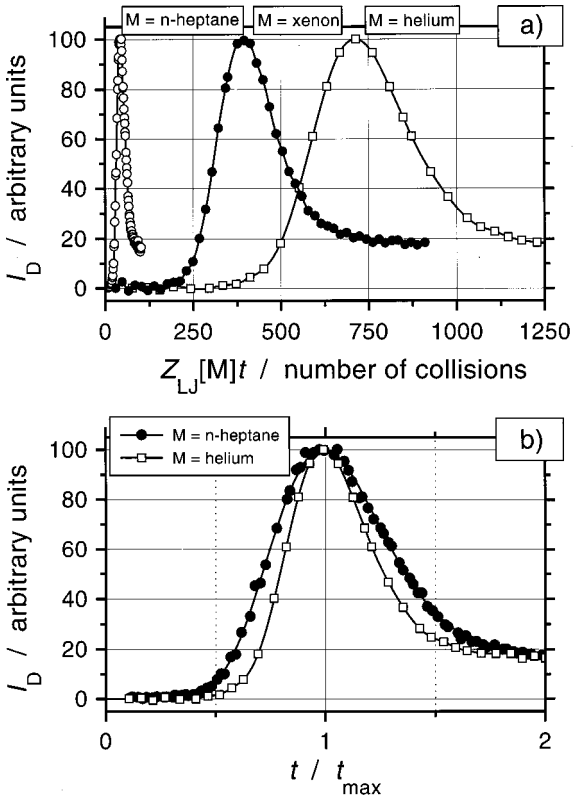

FIG. 9. (a) KCSI signals for toluene colliding with different bath gases, colliders: helium, xenon, and *n*-heptane; (b) relative widths of KCSI signals for the deactivation of toluene by helium and *n*-heptane; double normalized representation (maxima on top of each other). In all cases, pump $\lambda_0 = 266$ nm, probe $\lambda_1 = \lambda_2 = 275$ nm ($E_{center} = 3041\ cm^{-1}$). Lines intended only as a guide for the eye.

from critical data or on basis of a reference substance (e.g., toluene in the case of CHT) by using atomic, structural or group increment tables.[24,32]

V. QUALITATIVE ASPECTS OF KCSI SIGNALS

In this section we will discuss some additional basic features of KCSI signals to demonstrate that comprehensive information on the CET process can be easily extracted from the experiments by direct inspection without going into a detailed master equation analysis. We will also show, how basic CET quantities (with a quality comparable with results extracted, e.g., from corresponding UVA experiments) can already be obtained directly from the KCSI curves by an extremely simple and straightforward arrival time analysis ''using a ruler and a pencil.''

A. Pressure dependence

The upper plot in Fig. 8 shows KCSI signals for the deactivation of toluene by *n*-heptane measured at various pressures [probe wavelength $\lambda_1 = \lambda_2 = 275$ nm ($E_{center} = 3041\ cm^{-1}$)] normalized at their maximum value. As expected, the deactivation time (arrival and passing time at the observation window) increases with decreasing pressure. By simply scaling the time axis by the pressure and a collision number Z_{LJ} (Table I) one obtains the lower plot. Now, all curves fall exactly (within a fraction of a point size) on top of each other. This proves directly that one is observing solely collisional deactivation all the way down in the electronic ground state without side channel. An additional competing process partially or fully independent of pressure, as, e.g., deactivation via a triplet surface or a reactive process, would manifest itself in deviations between at least parts of the individual KCSI signals after the rescaling procedure.

B. Different colliders

The comparison of KCSI signals at a given observation window for the deactivation in different bath gases shows large variations in the number of collisions required for reaching the maximum ion signal. This is demonstrated in Fig. 9(a) with KCSI signals for the deactivation of toluene by helium, xenon, and *n*-heptane at the probe wavelength 275 nm ($E_{center} = 3041\ cm^{-1}$). The various arrival times of the curves—taken, e.g., as half the maximum value—directly correspond to the different efficiency of the colliders. The relative order of deactivating efficiency among the various monoatomic or polyatomic bath gases is immediately visible in an unquestionably very discriminative way.

Moreover, the width (or steepness of the leading edge) of a KCSI signal is highly sensitive to the nature of the

TABLE II. Energy transfer parameters $\overline{\langle \Delta E \rangle}$ and $\overline{\langle \Delta E^2 \rangle}$ from a simple arrival time analysis of KCSI signals for the deactivation of highly excited toluene by selected collider gases M (probe wavelength $\lambda_1 = 279$ nm). The results were obtained from Eq. (22) using $\langle E \rangle_0 = 49\,380\ \mathrm{cm}^{-1}$ and $E_{\mathrm{center}} = 3650\ \mathrm{cm}^{-1}$ (rectangular observation window from Paper II). $Zt_{\max}$ is the number of collisions, where the maximum of the KCSI curve appears. For comparison $\overline{\langle \Delta E \rangle}$ values from UVA experiments are given (Ref. 32). Note that the excitation energy of the UVA experiments is about $52\,000\ \mathrm{cm}^{-1}$ and that the (estimated) lower limit for these experiments (due to the method of data evaluation used in Ref. 32) is approximately $6000\ \mathrm{cm}^{-1}$ (see also Paper II). There are no other experimental values for $\overline{\langle \Delta E^2 \rangle}$ to compare with.

M	$Zt_{\max}$	$-\overline{\langle \Delta E \rangle}$ (KCSI) (cm^{-1})	$\overline{\langle \Delta E^2 \rangle}^{1/2}$ (KCSI) (cm^{-1})	$-\overline{\langle \Delta E \rangle}$ (UVA) (cm^{-1})
He	672	68	257	75
Ar	398	115	360	130
CO_2	195	235	602	280
cyclopropane	87.3	524	894	500

collider. To demonstrate this feature it is better to switch to a double normalized representation which puts the maxima of KCSI curves on top of each other, as done in Fig. 9(b), where a comparison for the bath gases helium and *n*-heptane is shown. It turns out that the relative slope of the leading edge becomes flatter with increasing size of the collider, i.e., the relative width of the KCSI curve increases; in other words it takes longer for the relaxing ensemble to pass through the observation window. This relative width of the KCSI curves is thus a direct measure of the width of the population distribution $g(E)$ passing the observation window during collisional deactivation—therefore characterizing $\langle \Delta E^2 \rangle$ [or, more general, the width of the underlying transition probability $P(E',E)$ generating $g(E,t)$].

C. Arrival time analysis of the KCSI signals

The findings of Sec. V B can be easily put on a more quantitative basis. A quick look on the left side of the scheme in Fig. 1 immediately shows which information is necessary to extract approximate $\langle \Delta E \rangle$ values from a KCSI signal. Basically only three quantities are needed which are easily extractable. First, the excitation energy $\langle E \rangle_{t=0}$ which is unambigously defined as the sum of the average energy of the thermal Boltzmann distribution plus the pump photon energy (wavelength λ_0). Second, the mean energy E_{center} of the observation window, which in the crude picture employed here can be taken as a simple rectangle (in terms of Fig. 1, E_{center} then corresponds to the middle of the long gray stripe). Finally, one needs the number of collisions for deactivation from the excitation energy $\langle E \rangle_0$ down to E_{center}. It can easily be seen, that this corresponds to $Zt_{\max}$, which is exactly the number of collisions required to reach the maximum of the KCSI curve, i.e., the point of deactivation where the maximum of the relaxing population has just reached the middle of the observation window. $\langle \Delta E \rangle$ values averaged over the energy interval defined by the excitation energy $\langle E \rangle_0$ and the center of the observation window E_{center} are then obtained via

$$\overline{\langle \Delta E \rangle} = \frac{\langle E \rangle_0 - E_{\mathrm{center}}}{Zt_{\max}}. \tag{22}$$

$Zt_{\max}$ can be easily extracted from the curves using ''ruler and pencil.'' In Table II we present $\overline{\langle \Delta E \rangle}$ values calculated from our toluene signals for the probe wavelength $\lambda_1 = 279$ nm $[E_{\mathrm{center}}(\mathrm{rectangle}) = 3650\ \mathrm{cm}^{-1}]$ and compare them to the UVA results from Ref. 32. In this case, we have used the rectangular observation window functions from Paper II to obtain E_{center} in Eq. (22). Note however that essentially the same $\overline{\langle \Delta E \rangle}$ values are obtained when using E_{center} from window functions which can be directly calculated from photophysical properties of the toluene molecule (see, e.g., the prescription as already given in Sec. III A and Paper II).

Although the arrival time analysis of the KCSI data are extremely simple, it can already provide the same information as is at best available from the toluene UVA measurements in Ref. 32. The agreement is very good. Clearly, KCSI signals contain much more information. The slope/width of the KCSI signals are directly correlated with the second moment $\langle \Delta E^2 \rangle$. A slightly more elaborate extension of the arrival time analysis—which is not further discussed at this point—allows us to calculate $\overline{\langle \Delta E^2 \rangle}$ (i.e., $\langle \Delta E^2 \rangle$ averaged over the same energy interval as $\overline{\langle \Delta E \rangle}$) directly from the slope of the KCSI curve's leading edge. The values from this analysis are also included in Table II. To exploit the full CET information in the KCSI signals it is however necessary to proceed with a detailed master equation analysis which is outlined in the following.

VI. MASTER EQUATION ANALYSIS OF KCSI SIGNALS

While a full account of our toluene and azulene results will be given in Paper II (following article) and Ref. 67, at this point we will not go into the specific details of an elaborate parameter analysis. Instead, we will highlight briefly some important general findings common to the master equation simulations. A brief summary of the formalism has already been given in Sec. III B. There is no way to extract the ''real'' functional form of $P(E',E)$ by direct deconvolution of Eq. (5), due to the finite accuracy of the experimental data and the collision cascade character of the relaxation. This will be discussed in detail in Paper II. Instead, specific analytical test functions for $P(E',E)$ are assumed, and the parameters for the best global fit of the experimental data with such functions are determined by a master equation analysis.

Which degree of uniqueness of a ''best fit'' can one expect if there may exist too many physically distinct possibilities to fit our data? This issue—of great concern in the beginning of our simulation efforts—proved itself to be not serious at all. On the contrary, it was experienced in time consuming attempts how tightly bound the conditions for successful modeling were. Simultaneous fitting of, e.g., six independent KCSI curves for the system azulene $+n$-heptane (Fig. 3), each of which represents a mathematically complex function with variations of the position and shape of its main structure, differs substantially from, e.g., the common problem of fitting a few monotonously decaying curves. As a general result an amazing degree of uniqueness was found. We illustrate only one step in that direction. If

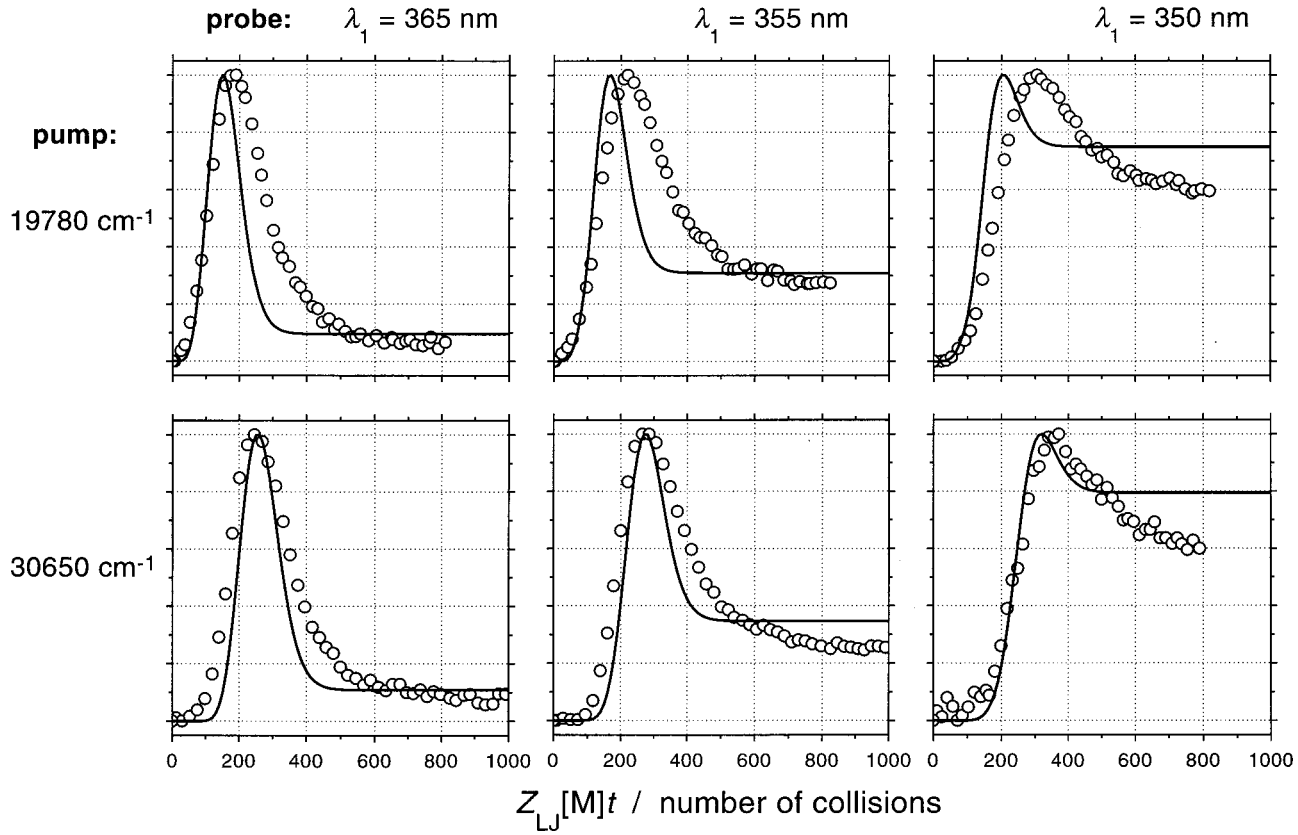

FIG. 10. Same as Fig. 3, but for the collider argon and master equation fit (solid line) calculated using a monoexponential transition probability of the form $P(E',E) \propto \exp[-(E-E')/\alpha]$ with energy *independent* parameter $\alpha = 225\ \mathrm{cm}^{-1}$; for details, see text.

one assumes, e.g., any exponential form $P(E',E) \propto \exp[-(E-E')/\alpha]$ with constant (=energy independent) α, as it is still often found in theoretical discussions, then this will allow to model—at best—*one* correct position of a maximum out of *six* KCSI curves while at the same time a strong mismatch for the five others cannot be avoided. This is illustrated in Fig. 10 for our azulene+argon measurements where only for the signal at $\lambda_1 = 355\,\mathrm{nm}$ and 30650 cm^{-1} excitation energy the maxima of the simulated and experimental curves coincide. In addition, completely wrong *shapes* for all six signals are unavoidable, as is also an incorrect final level of the ion signal after complete deactivation in every single curve. Very similar results are obtained in our toluene experiments (Paper II). Therefore, it is clearly necessary to go beyond a simple, purely monoexponential representation of $P(E',E)$ with energy independent denominator. This is done in the solid line simulations already shown for the azulene+*n*-heptane case in Fig. 3 which represent the optimized fits very close to the limits of experimental accuracy which is reached within a class of monoexponential functions for $P(E',E)$ with a parametric exponent Y in the argument, i.e., $P(E',E) \propto \exp[-((E-E')/\alpha_1)^Y]$, including energy dependent $\alpha_1(E)$. As a consequence, only a very restricted set of possible $P(E',E)$ test functions with well-defined parameters can successfully describe the experimental data for the various molecules and bath gases; all of them leading, e.g., to a approximately linear dependence of the first moment of energy transfer $\langle \Delta E \rangle$. For a detailed discussion of this issue in the toluene system, see Paper II.

VII. CONCLUSIONS

As an experimental technique to study CET in polyatomic molecules kinetically controlled selective ionization (KCSI) allows to extract complete sets of transition probabilities $P(E',E)$ and the corresponding moments of energy transfer $\langle \Delta E^n \rangle$ even at quasicontinuous densities of states. The method itself and its experimental realization have been discussed in detail. Basic information on CET can already be extracted from the data by applying a simple analysis of the arrival times and the width of the experimental curves. The formalism of the master equation treatment was sketched which serves as the basis of a complete data evaluation. Selected examples of KCSI experiments on collisional relaxation were discussed. These yield important aspects of the quality and the general character of $P(E',E)$ parameters, which are for the first time completely accessible by this method. They show that the bounds for successful modeling of KCSI curves are tight and restricted. Parameters deduced from KCSI measurements therefore represent a high level of accuracy and certainty and may be used as benchmark results for thorough tests of trajectory calculations and future CET theories.

ACKNOWLEDGMENTS

We thank Jürgen Troe for valuable comments and Uwe Grigoleit for his help. This work has been financially supported by the Deutsche Forschungsgemeinschaft [SFB 93

(''Photochemie mit Lasern,'' C16) and SFB 357 (''Molekulare Mechanismen unimolekularer Prozesse,'' A7)].

[1] D. C. Tardy and B. S. Rabinovitch, Chem. Rev. **77**, 396 (1977).
[2] H. Hippler and J. Troe, in *Bimolecular Collisions*, edited by J. E. Baggott and M. N. R. Ashfold (The Royal Society of Chemistry, London, 1989), p. 209.
[3] M. Quack and J. Troe, in *Gas Kinetics and Energy Transfer*, edited by P. G. Ashmore and R. J. Donovan (The Chemical Society, London, 1977), Vol. 2.
[4] I. Oref and D. C. Tardy, Chem. Rev. **90**, 1407 (1990).
[5] R. E. Weston Jr. and G. W. Flynn, Annu. Rev. Phys. Chem. **43**, 559 (1992).
[6] G. W. Flynn, C. S. Parmenter, and A. M. Wodtke, J. Phys. Chem. **100**, 12817 (1996).
[7] T. Lenzer, K. Luther, J. Troe, R. G. Gilbert, and K. F. Lim, J. Chem. Phys. **103**, 626 (1995).
[8] T. Lenzer and K. Luther, Ber. Bunsenges. Phys. Chem. **101**, 581 (1997).
[9] J. R. Barker, Ber. Bunsenges. Phys. Chem. **101**, 566 (1997).
[10] S. Nordholm, L. E. B. Börjesson, L. Ming, and H. Svedung, Ber. Bunsenges. Phys. Chem. **101**, 574 (1997).
[11] K. F. Lim and R. G. Gilbert, J. Phys. Chem. **94**, 72 (1990).
[12] K. F. Lim and R. G. Gilbert, J. Phys. Chem. **94**, 77 (1990).
[13] V. Bernshtein and I. Oref, J. Chem. Phys. **104**, 1958 (1996).
[14] V. Bernshtein and I. Oref, Chem. Phys. Lett. **233**, 173 (1995).
[15] M. Bruehl and G. C. Schatz, J. Phys. Chem. **92**, 3190 (1988).
[16] G. Lendvay and G. C. Schatz, J. Chem. Phys. **96**, 4356 (1992).
[17] G. Lendvay and G. C. Schatz, J. Chem. Phys. **98**, 1034 (1993).
[18] G. Lendvay and G. C. Schatz, in *Vibrational Energy Transfer Involving Large and Small Molecules*, edited by J. R. Barker, Advances in Chemical Kinetics and Dynamics, Vol. 2B (JAI, Greenwich, CT, 1995), pp. 481–513.
[19] G. Lendvay, J. Phys. Chem. A **101**, 9217 (1997).
[20] G. C. Schatz and G. Lendvay, J. Chem. Phys. **106**, 3548 (1997).
[21] T. Lenzer and K. Luther, J. Chem. Phys. **105**, 10944 (1996).
[22] U. Hold, T. Lenzer, K. Luther, K. Reihs, and A. C. Symonds, Ber. Bunsenges. Phys. Chem. **101**, 552 (1997).
[23] K. Luther and K. Reihs, Ber. Bunsenges. Phys. Chem. **92**, 442 (1988).
[24] K. Reihs, Ph.D. thesis, University of Göttingen, 1989.
[25] S. Hassoon, I. Oref, and C. Steel, J. Chem. Phys. **89**, 1743 (1989).
[26] J. M. Morgulis, S. S. Sapers, C. Steel, and I. Oref, J. Chem. Phys. **90**, 923 (1990).
[27] A. S. Mullin, C. A. Michaels, and G. W. Flynn, J. Chem. Phys. **102**, 6682 (1995).
[28] C. A. Michaels and G. W. Flynn, J. Chem. Phys. **106**, 3558 (1997).
[29] N. J. Brown and J. A. Miller, J. Chem. Phys. **80**, 5568 (1984).
[30] G. Lendvay and G. C. Schatz, J. Phys. Chem. **98**, 6530 (1994).
[31] H. Hippler, J. Troe, and H. J. Wendelken, Chem. Phys. Lett. **84**, 257 (1981).
[32] H. Hippler, J. Troe, and H. J. Wendelken, J. Chem. Phys. **78**, 6709 (1983).
[33] M. Damm, F. Deckert, H. Hippler, and J. Troe, J. Phys. Chem. **95**, 2005 (1991).
[34] M. Damm, F. Deckert, and H. Hippler, Ber. Bunsenges. Phys. Chem. **101**, 1901 (1997).
[35] G. P. Smith and J. R. Barker, Chem. Phys. Lett. **78**, 253 (1981).
[36] M. J. Rossi, J. R. Pladziewicz, and J. R. Barker, J. Chem. Phys. **78**, 6695 (1983).
[37] J. D. Brenner, J. P. Erinjeri, and J. R. Barker, Chem. Phys. **175**, 99 (1993).
[38] L. A. Miller and J. R. Barker, J. Chem. Phys. **105**, 1383 (1996).
[39] L. A. Miller, C. D. Cook, and J. R. Barker, J. Chem. Phys. **105**, 3012 (1996).
[40] J. R. Gascooke, Z. T. Alwahabi, K. D. King, and W. D. Lawrance, J. Chem. Phys. **109**, 3868 (1998).
[41] E. A. Coronado and J. C. Ferrero, J. Phys. Chem. A **101**, 9603 (1997).
[42] W. Braun, M. D. Scheer, and V. Kaufman, J. Res. Natl. Bur. Stand. **91**, 313 (1986).
[43] T. J. Wallington, M. D. Scheer, and W. Braun, Chem. Phys. Lett. **138**, 538 (1987).
[44] W. Braun, M. D. Scheer, and R. J. Cvetanovic, J. Chem. Phys. **88**, 3715 (1988).
[45] K. M. Beck, A. Ringwelski, and R. J. Gordon, Chem. Phys. Lett. **121**, 529 (1985).
[46] A. Karbach and P. Hess, J. Chem. Phys. **84**, 2945 (1986).
[47] K. M. Beck and R. J. Gordon, J. Chem. Phys. **87**, 5681 (1987).
[48] J. R. Barker and T. Rothem, Chem. Phys. **68**, 331 (1982).
[49] B. M. Toselli, T. L. Walunas, and J. R. Barker, J. Chem. Phys. **92**, 4793 (1990).
[50] A. Chimbayo, B. M. Toselli, and J. R. Barker, Chem. Phys. Lett. **259**, 225 (1996).
[51] A. Chimbayo, B. M. Toselli, and J. R. Barker, J. Chem. Phys. **108**, 2383 (1998).
[52] G. V. Hartland, D. Qin, and H.-L. Dai, J. Chem. Phys. **101**, 8554 (1994).
[53] G. V. Hartland, D. Qin, and H.-L. Dai, J. Chem. Phys. **102**, 8677 (1995).
[54] C. D. Pibel, E. Sirota, J. Brenner, and H.-L. Dai, J. Chem. Phys. **108**, 1297 (1998).
[55] C. A. Michaels, A. S. Mullin, J. Park, J. Z. Chou, and G. W. Flynn, J. Chem. Phys. **108**, 2744 (1998).
[56] M. C. Wall, B. A. Stewart, and A. S. Mullin, J. Chem. Phys. **108**, 6185 (1998).
[57] M. C. Wall and A. S. Mullin, J. Chem. Phys. **108**, 9658 (1998).
[58] M. C. Wall, A. S. Lemoff, and A. S. Mullin, J. Phys. Chem. A **102**, 9101 (1998).
[59] M. Fraelich, M. S. Elioff, and A. S. Mullin, J. Phys. Chem. A **102**, 9761 (1998).
[60] M. S. Elioff, M. C. Wall, A. S. Lemoff, and A. S. Mullin, J. Chem. Phys. **110**, 5578 (1999).
[61] J. Z. Chou, S. A. Hewitt, J. F. Hershberger, B. B. Brady, G. B. Spector, L. Chia, and G. W. Flynn, J. Chem. Phys. **91**, 5392 (1989).
[62] G. W. Flynn and R. E. Weston Jr., J. Phys. Chem. **97**, 8116 (1993).
[63] H.-G. Löhmannsröben and K. Luther, Chem. Phys. Lett. **144**, 473 (1988).
[64] (a) T. Lenzer, K. Luther, U. Hold, and A. C. Symonds, Springer Proc. Phys. **68**, 237 (1992); (b) T. Lenzer, K. Luther, Karsten Reihs, and Andrew C. Symonds, J. Chem. Phys. **112**, 4090 (2000), following paper.
[65] U. Hold, Ph.D. thesis, University of Göttingen, 1994.
[66] A. C. Symonds, Ph.D. thesis, University of Göttingen, 1992.
[67] U. Grigoleit, U. Hold, T. Lenzer, K. Luther, K. Reihs, and A. C. Symonds, J. Chem. Phys. (to be submitted).
[68] U. Grigoleit, Ph.D. thesis, University of Göttingen, 1999.
[69] U. Grigoleit, T. Lenzer, and K. Luther (unpublished).
[70] W. K. Bischel, L. J. Jusinski, M. N. Spencer, and D. J. Eckstrom, J. Opt. Soc. Am. B **2**, 877 (1985).
[71] R. G. Gilbert and S. C. Smith, *Theory of Unimolecular and Recombination Reactions* (Blackwell Scientific, Oxford, 1990).
[72] R. G. Gilbert and K. D. King, Chem. Phys. **49**, 367 (1980).
[73] R. G. Gilbert, K. Luther, and J. Troe, Ber. Bunsenges. Phys. Chem. **87**, 169 (1983).
[74] G. Z. Whitten and B. S. Rabinovitch, J. Chem. Phys. **38**, 2466 (1963).
[75] G. Z. Whitten and B. S. Rabinovitch, J. Chem. Phys. **41**, 1883 (1964).
[76] G. Varsany, *Assignment for Vibrational Spectra of 700 Benzene Derivatives* (Akademiai Kaido, Budapest, 1973).
[77] H. D. Rudolph, H. Dreizler, A. Jaeschke, and P. Wendling, Z. Naturforsch. A **22a**, 940 (1967).
[78] T. Beyer and D. F. Swinehart, Comm. Assoc. Comput. Machines **16**, 379 (1973).
[79] S. E. Stein and B. S. Rabinovitch, J. Chem. Phys. **58**, 2438 (1973).
[80] B. M. Toselli, J. D. Brenner, M. L. Yerram, W. E. Chin, K. D. King, and J. R. Barker, J. Chem. Phys. **95**, 176 (1991).
[81] V. S. Lethokov, V. I. Mishin, and A. A. Puretzsky, Prog. Quantum Electron. **5**, 139 (1977).
[82] H.-G. Löhmannsröben, Ph.D. thesis, University of Göttingen, 1985.
[83] U. Boesl, H. J. Neusser, and E. W. Schlag, Chem. Phys. **55**, 193 (1981).